International Journal of Minerals, Metallurgy and Materials
Volume 27, Number 10, October 2020, Page 1347
https://doi.org/10.1007/s12613-020-2028-x

A new method of preparing high-performance high-entropy alloys through high-gravity combustion synthesis

Fu-kai Zheng[1,2)], *Guan-nan Zhang*[3)], *Xiu-juan Chen*[1,2)], *Xiao Yang*[3)], *Zeng-chao Yang*[3)], *Yong Li*[3)], *and Jiang-tao Li*[3)]

1) College of Materials Science and Engineering, Lanzhou University of Technology, Lanzhou 730050, China
2) College of Mechano-Electronic Engineering, Lanzhou University of Technology, Lanzhou 730050, China
3) Key Laboratory of Cryogenics, Technical Institute of Physics and Chemistry, Chinese Academy of Sciences, Beijing 100190, China
(Received: 24 December 2019; revised: 23 February 2020; accepted: 24 February 2020)

Abstract: A new method of high-gravity combustion synthesis (HGCS) followed by post-treatment (PT) is reported for preparing high-performance high-entropy alloys (HEAs), $Cr_{0.9}FeNi_{2.5}V_{0.2}Al_{0.5}$ alloy, whereby cheap thermite powder is used as the raw material. In this process, the HEA melt and the ceramic melt are rapidly formed by a strong exothermic combustion synthesis reaction and completely separated under a high-gravity field. Then, the master alloy is obtained after cooling. Subsequently, the master alloy is sequentially subjected to conventional vacuum arc melting (VAM), homogenization treatment, cold rolling, and annealing treatment to realize a tensile strength, yield strength, and elongation of 1250 MPa, 1075 MPa, and 2.9%, respectively. The present method is increasingly attractive due to its low cost of raw materials and the intermediate product obtained without high-temperature heating. Based on the calculation of phase separation kinetics in the high-temperature melt, it is expected that the final alloys with high performance can be prepared directly across master alloys with higher high-gravity coefficients.

Keywords: high-entropy alloys; high gravity; combustion synthesis; post-treatment; low-cost; high performance

1. Introduction

High-entropy alloys (HEAs) have received extensive attention due to their special composition and microstructure [1–7]. For a long time, most studies have focused on realizing excellent mechanical properties. In particular, $Cr_{0.9}FeNi_{2.5}V_{0.2}Al_{0.5}$ alloy with good plasticity and ultrahigh yield strength up to 1700–1900 MPa has been explored based on precipitation strengthening mechanism [8]. In general, arc melting, induction melting, mechanical alloying, electrochemical deposition, laser cladding, and many other conventional preparation methods have been adopted to fabricate HEAs. However, to obtain the excellent properties of the material, the expensive high-purity metals such as Cr, Ni, and V must be used as raw materials, which results in high manufacturing cost and serious restrictions in engineering applications. Therefore, to promote the practical use of HEAs, reducing the production cost is necessary, and this requires the development of a new material preparation technology that is not dependent to expensive metal materials.

A corresponding metal can be obtained by a redox reaction between a metal oxide powder and an aluminum powder, and this mixture of metal oxide powder and aluminum powder is called a thermite [9–10]. Since as early as 20th century, the technology has been successfully applied to the welding of train tracks by iron melt, which is formed from the reaction of Al + Fe_2O_3 thermite. With the development of high-speed rail technology, the oxide composition in thermite for rail welding has also expanded from a single iron oxide to a variety of oxide powders, including nickel oxide and vanadium oxide, which will enable the alloying of the weld bead and improve the performance of weld bead. Due to the successful industrial application of thermites, an HEA with the desired composition can be obtained through the reasonable component design of different thermite systems. In addition, since the cost of the metal oxide raw material is much lower than that of the corresponding high-purity metal raw material, a low-cost preparation of HEA can be realized by rationally utilizing the combustion reaction of thermite.

The above assumption is feasible in principle. However,

Corresponding authors: Xiu-juan Chen E-mail: chenxj@lut.cn; Xiao Yang E-mail: yangxiao@mail.ipc.ac.cn

after a multi-component thermite undergoes a strong exothermic combustion reaction, the product is a mixed melt of ceramic and metal, but both of them can be separated due to density differences under the earth gravitational field. The degree of separation depends on the melt viscosity. Considering that the window period of the high-temperature melt produced by the strong exothermic reaction is short, an additional strong field must be applied to the reaction system to enhance the transport efficiency of substance and energy in the melt, fully separate the ceramic phase from the metal melt, and finally obtain a dense non-inclusion HEA, which could speed up the phase separation.

To solve the above problems, we have proposed a high-gravity field in the reaction system during the thermite reaction, based on a method called high-gravity combustion synthesis (HGCS). The density difference between the different phases is utilized to accelerate the separation of the Al_2O_3 ceramics and bubbles from the molten metal in the high-gravity field, thereby achieving a dense and non-inclusion metal melt in the subsequent solidification. The process has been proven to be feasible in the preparation of pure Cu, pure Ni, single-phase HEAs, and composites [11–15]. However, whether the process is equally applicable to high-strength and tough HEAs, based on precipitated strengthening mechanism, needs to be verified.

Based on the above introduction, the present study aims to fabricate $Cr_{0.9}FeNi_{2.5}V_{0.2}Al_{0.5}$ master alloy using thermite consisting of Al powder and oxide ceramic powders as the raw material through HGCS. A pure and dense alloy ingot is obtained by successively subjecting the master alloy to vacuum arc melting (VAM), homogenizing treatment, cold rolling, and aging treatment. Compared with the traditional VAM process, the HGCS combined with the vacuum arc remelting process may be a more efficient and cheaper method for HEA preparation.

2. Experimental

2.1. Alloys preparation

Commercial powders of Cr_2O_3, Fe_2O_3, NiO, V_2O_3, and Al with a particle size of less than 74 μm were used as raw materials. The Al powder had a purity of >99wt%, and others were analytical-grade reagents. To obtain the designed alloy samples, the dried ceramic powder and Al powder were fully mixed to prepare a thermite according to the stoichiometric ratio of the following reaction:

$$\frac{9}{20}Cr_2O_3+\frac{1}{2}Fe_2O_3+\frac{5}{2}NiO+\frac{1}{10}V_2O_3+\frac{64}{15}Al \xrightarrow{\text{Ignition}} Cr_{0.9}FeNi_{2.5}V_{0.2}Al_{0.5}+\frac{113}{60}Al_2O_3 \quad (1)$$

The thermite powder was cold-pressed into cylindrical solid with a diameter of 40 mm and a porosity of nearly 50%, which was then loaded into a reaction mold. Afterward, the reaction mold was horizontally mounted at one side of a rotator in the reaction chamber. The counterweight was mounted at the other side of the rotator to maintain dynamic balance. The schematic illustration of the raw material assembly and equipment is shown in Fig. 1(a).

The reaction chamber was evacuated to a vacuum of nearly 100 Pa; then, the rotator began to rotate, and the high-gravity field was generated by centrifugation effect. When the centrifugal acceleration (g') was 1500g (g = 9.8 m/s^2, normal gravitational acceleration), the thermite was induced by heating the tungsten wire to carry out the combustion synthesis reaction. During the reaction, molten alumina and metallic melt formed rapidly and were quickly separated from each other using the high-gravity field. After solidification, the final product consisted of two distinct layers: bulk Al_2O_3 and designed $Cr_{0.9}FeNi_{2.5}V_{0.2}Al_{0.5}$ HEA. A brief illustration of the HGCS of this alloy is shown in Fig. 1(b).

To eliminate pores and inclusions, the synthesized alloys were remelted by traditional VAM using high-purity metal as raw materials. Considering the needs of the comparative experiment, $Cr_{0.9}FeNi_{2.5}V_{0.2}Al_{0.5}$ alloy ingots were prepared by vacuum arc-melting pure metals (Cr, Fe, Ni, V, and Al with purity > 99.9wt%).

2.2. Post-treatment (PT)

To reduce component segregation, the prepared alloy ingots were homogenized at 1200°C for 20 h, followed by water quenching. Homogenized alloys were then subjected to multi-pass cold rolling to about 60% reduction in thickness and then aging at 700°C for 1 h, followed by air cooling.

2.3. Structure characterization and tensile test

The crystal structure was analyzed by X-ray diffraction (XRD) (model D8/ADVANCE, Bruker, Germany) with a step of 0.02° and a scanning rate of 0.05°/s. The microstructure was characterized using scanning electron microscopy (SEM, model S-4800, Hitachi, Japan) equipped with energy-dispersive spectroscopy (EDS). Tensile tests were performed by a CMT4305 universal electronic tensile testing machine at room temperature with a nominal strain rate of 5×10^{-3} s^{-1}.

3. Results and discussion

The XRD analysis (Fig. 1(c)) shows the evolution of the crystalline structure of $Cr_{0.9}FeNi_{2.5}V_{0.2}Al_{0.5}$ alloy during the preparation. The samples in different stages mainly formed face-centered-cubic (fcc) solid solution phase, indicating that the high-entropy stabilized phase had been formed by HGCS, and it exhibited good structural stability during VAM and PT. In addition, fine diffraction peaks of ordered phases were observed on the diffraction patterns of the alloy prepared by HGCS and that prepared by HGCS combined with VAM. However, the ordered phase disappeared in the alloy after PT,

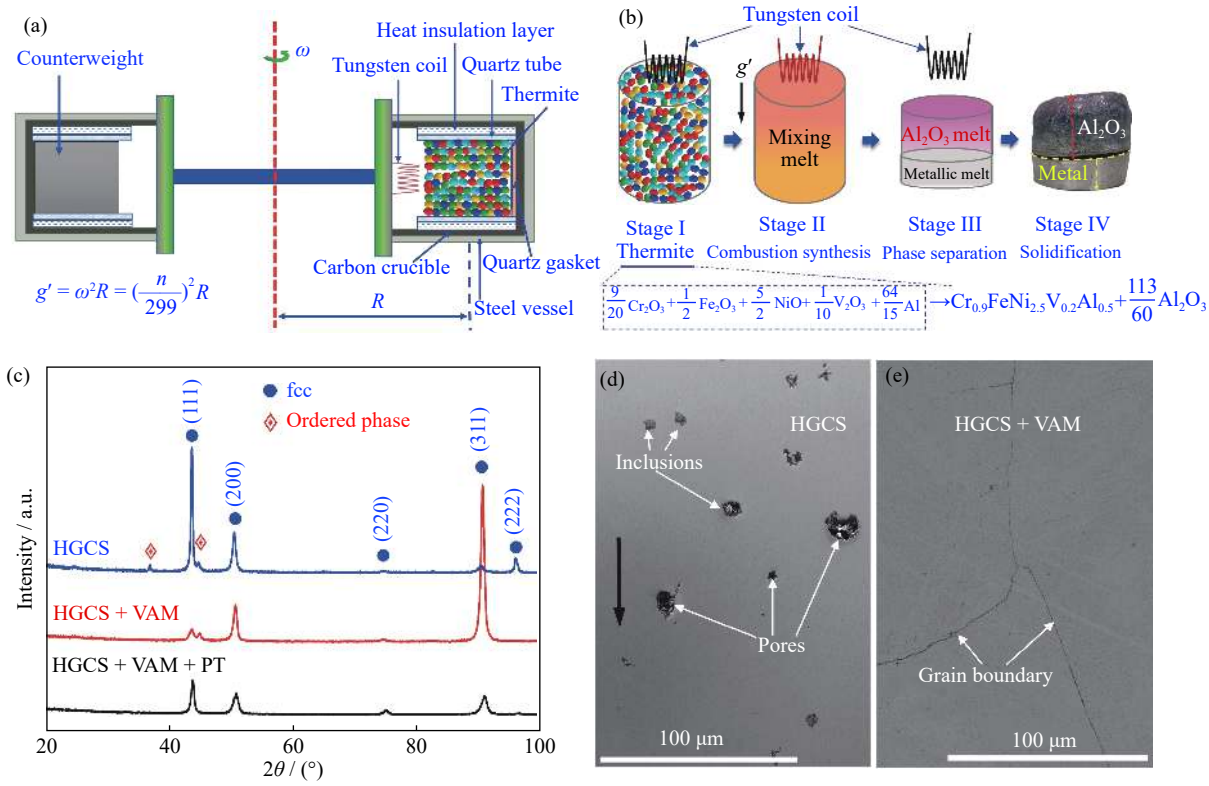

Fig. 1. Process of preparing HEA by high-gravity combustion synthesis and the characteristics of prepared samples: (a) schematic illustration of raw material assembly and equipment; (b) brief illustration of the HGCS of $Cr_{0.9}FeNi_{2.5}V_{0.2}Al_{0.5}$ alloy; (c) XRD patterns of samples at different stages of alloy preparation; (d, e) the microstructure of HGCS specimen and HGCS combined with vacuum arc-melted specimen (HGCS + VAM), respectively. HGCS + VAM + PT represents samples subjected to high-gravity combustion synthesis, vacuum arc melting, and post-treatment in sequence. ω denotes the angular velocity of the rotor, and R denotes the vertical distance from rotor to motor shaft.

indicating that PT may lead to the reconstruction of the alloy microstructure.

Figs. 1(d) and 1(e) present the microstructures of the HGCS specimen and HGCS + VAM specimen, respectively. A large number of inclusions and pores were found in the high-gravity combustion synthesized alloy, which will be eliminated during VAM, and a dense equiaxed crystal structure with a size of approximately several hundred microns was formed.

PT was performed to obtain excellent comprehensive mechanical properties. As shown in Fig. 2(a), the final alloy sequentially subjected to HGCS, VAM, and PT (marked as HGCS + VAM + PT) exhibited high tensile strength and remarkable ductility. The tensile yield strength ($\sigma_{0.2}$), tensile fracture strength (σ_f), and plastic elongation (ε) of the alloy reached 1075 MPa, 1250 MPa, and 2.9%, respectively. For comparison, $Cr_{0.9}FeNi_{2.5}V_{0.2}Al_{0.5}$ alloy was prepared by VAM using high-purity metal as raw materials and was then subjected to the same PT, marked as VAM + PT. The tensile mechanical properties of the $Cr_{0.9}FeNi_{2.5}V_{0.2}Al_{0.5}$ HEA were also tested and demonstrated in Fig. 2(a). The mechanical properties of the HGCS + VAM + PT alloy were close to those of the VAM + PT alloy. The detailed mechanical performance data are listed in Table 1. In addition, two alloys in this work also displayed similar work-hardening behavior (represented by the dotted lines in Fig. 2(a)). With the increase in uniform strain, the strain-hardening rate continued to decrease until local stress concentration occurred, resulting in catastrophic fracture. However, the strengths and ductility of the alloys reported in this work are significantly lower than the results reported in the literature [8], which may be due to different cold rolling reductions.

Fig. 2(b) shows the macroscopic morphology of the HGCS + VAM + PT alloy fracture surface. From the center to the edge, three different areas are shown: I, II, and III. In region I (Fig. 2(c)), abundant dimples with a diameter of 1–5 μm were observed, indicating large plastic deformation. In region II (Fig. 2(d)), the fracture surface was relatively smooth, and traces of relative slip existed between crystals, which is a characteristic of rapid crack propagation. In region III (Fig. 2(e)), the specimen tore quickly, resulting in a rough surface and a large number of cracks.

The deformation mechanism of the alloy is the local micropore aggregation growth mechanism, which is related to the alloy microstructure. As presented in Figs. 2(f) and 2(g), the HGCS + VAM + PT alloy exhibited phase separation. A

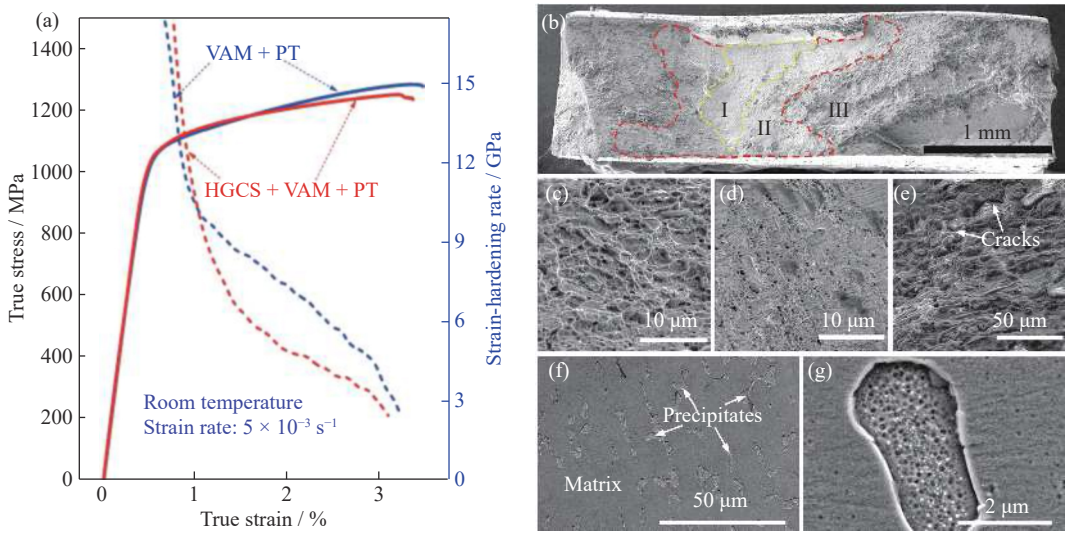

Fig. 2. Mechanical properties and macroscopic morphology of $Cr_{0.9}FeNi_{2.5}V_{0.2}Al_{0.5}$ HEA: (a) true stress–strain curve (solid line) and work-hardening behavior (dotted line) of HEA at room temperature; (b) the macroscopic morphology of the fracture surface for HGCS + VAM + PT alloy; (c)–(e) dimple zone, slip zone, and tear zone corresponding to the three different regions from the center to the edge—I, II, and III in (a), respectively; (f, g) SEM micrographs of HGCS + VAM + PT alloy.

Table 1. Tensile mechanical properties of $Cr_{0.9}FeNi_{2.5}V_{0.2}Al_{0.5}$ HEA in this work and Ref. [8] at room temperature

Alloys	$\sigma_{0.2}$ / MPa	σ_f / MPa	ε / %
HGCS + VAM + PT	1075	1250	2.9
VAM + PT	1073	1282	3.0
Ref. [8]	1570	1763	10.0

large number of nano-precipitates with an average grain size of about 50 nm were preferentially precipitated and aggregated in certain regions and were distributed on the matrix in the form of clusters. According to the EDS data of the corresponding region listed in Table 2 and similar reported results in Ref. [8], nano-precipitates and the matrix are inferred to be ordered $L1_2$ phases and fcc-structured disorder solid solution phases, respectively. The microstructure inhomogeneity led to local stress concentration in the sample under external loading.

In summary, the presented method has been proved to have the potential to produce high performance HEAs at a low cost. Realizing complete phase separation (ceramic phase and bubbles escape from the metal melt) during HGCS can enable the direct preparation of high-purity metal without remelting, which is of great value for simplifying the process. Thus, the phase separation process is discussed based on a simple model as follows.

Table 2. Density, viscosity, and surface energy for alloyed elements, HEA melt, and Al_2O_3 ceramic and $C_{nominal}$ (at%, nominal composition of HGCS + VAM + PT alloy), C_{exp} (at%, experimentally measured composition of HGCS + VAM + PT alloy), C_{matrix} (at%, mean composition of matrix), and $C_{precipitation}$ (at%, mean composition of precipitation) of HEAs prepared by HGCS

Material or element	Density (ρ) / ($g \cdot cm^{-3}$)	Viscosity (η) / (Pa·s)	Surface energy (γ) / ($N \cdot m^{-1}$)	Composition			
				$C_{nominal}$ / at%	C_{exp} / at%	C_{matrix} / at%	$C_{precipitation}$ / at%
Cr	6.29	0.0057	1.70	17.65	18.89	16.06	12.16
Fe	7.03	0.0055	1.87	19.61	22.45	20.51	12.96
Ni	7.90	0.0049	1.78	49.02	45.55	50.68	53.00
V	5.36	0.0024	1.95	3.92	3.78	3.86	2.89
Al	2.38	0.0013	0.94	9.80	9.34	8.90	18.98
$Cr_{0.9}FeNi_{2.5}V_{0.2}Al_{0.5}$	6.58	0.0047	1.71	—	—	—	—
Al_2O_3	2.81 (melt), 3.99 (solid)	0.0300	0.64	—	—	—	—

According to Stokes' law, it is assumed that only three forces are applied to ceramic particles and gas bubbles in a metallic melt, which are high gravity (F_g), buoyant force (F_b), and viscous resistance (F_v), as shown in Fig. 3(a). The rising displacement of ceramic particles (L_C) and gas bubbles (L_B) in metallic melts can be deduced as follows:

$$L_C = \frac{2}{9}(\rho_{M,l} - \rho_{C,s})\frac{R_c^2 g'}{\eta_M}\left[t_{melt} - \frac{1}{9}(\rho_{M,l} - \rho_{C,s})\frac{R_c^2}{\eta_M}\right] \quad (2)$$

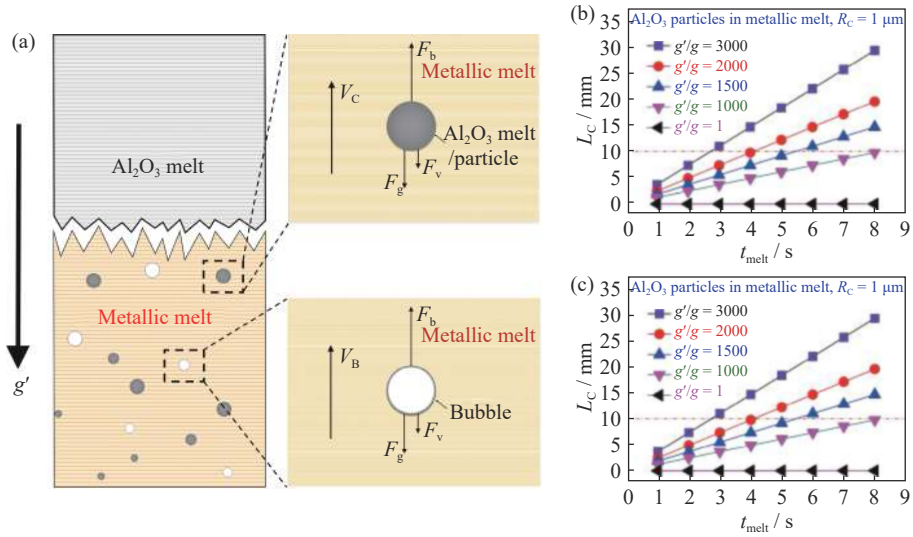

Fig. 3. Phase separation mechanism during high-gravity combustion synthesis: (a) schematic illustration of phase separation in metallic melt; (b) the relationship between the melt retention time and the rising displacement of ceramic particles in different high-gravity coefficients; (c) the relationship between the melt retention time and the rising displacement of gas bubbles under different high-gravity coefficients. V_C denotes the rising velocity of ceramic particles in metallic melts, V_B denotes the rising velocity of gas bubbles in metallic melts.

$$L_B = \frac{2}{9}\frac{\rho_{M,l}R_B^2 g'}{\eta_M}\left(t_{melt} - \frac{1}{9}\frac{\rho_{M,l}R_B^2}{\eta_M}\right) \quad (3)$$

where $\rho_{M,l}$ and $\rho_{C,s}$ denote the densities of the HEA melt and ceramic particle, respectively; g' denotes the centrifugal acceleration in high-gravity field; R_C and R_B denote the radii of the ceramic particle and gas bubble, respectively; η_M denotes the viscosity of the HEA melt, and t_{melt} denotes the HEA melt retention time.

With $R_C = R_B = 1$ μm and using the other available data listed in Table 2 [16–19], the L_C and L_B values under different high-gravity factors, g'/g, were calculated and are plotted in Figs. 3(b) and 3(c), respectively. The rising displacement of ceramic particles or gas bubbles is strongly dependent on high-gravity factors and the HEA melt retention time, which means that the strong high-gravity field and durable high-temperature melt will facilitate the discharge of ceramic inclusions and gas bubbles. The preliminary experimental results show that the cooling rate of the high-temperature melt was greater than 1000°C/s, and the adiabatic temperature, calculated from Eq. (1), is 2938 K. Thus, the HEA melt retention time is estimated to be 2–3 s. To obtain a high-purity dense HEA alloy ingot, the high-gravity factors are required to be greater than 3000, which is significantly higher than our experimental conditions, $g'/g = 1500$.

4. Conclusion

A master alloy of $Cr_{0.9}FeNi_{2.5}V_{0.2}Al_{0.5}$ HEA was prepared by HGCS and using the thermite Al powder + oxide ceramic powders as raw material. Subsequently, a dense, non-inclusion alloy sample could be obtained by subjecting this master alloy to sequential conventional vacuum arc remelting, homogenization treatment, cold rolling, and annealing treatment, leading to high comprehensive mechanical properties (tensile yield strength of 1075 MPa, tensile fracture strength of 1250 MPa, and plastic elongation of 2.9%). According to the kinetics analysis of phase separation in the high-temperature melt, the gravity coefficient and viscosity of the melt played a very important role in the densification and purification process of the alloy. The proposed method replaces expensive high-purity metals such as Cr, Ni, and V with cheap thermite powders as raw materials and provides a new approach for the low-cost production of high-performance HEAs.

Acknowledgements

This work was financially supported by the National Natural Science Foundation of China (No. 51702332), the Key Research Projects in Gansu Province (No. 17YF1GA020), the CAS Key Laboratory of Cryogenics, Technical Institute of Physics and Chemistry (Youth Innovation Fund No. CRYOQN201705).

References

[1] Z.F. Lei, X.J. Liu, Y. Wu, *et al.*, Enhanced strength and ductility in a high-entropy alloy via ordered oxygen complexes, *Nature*, 563(2018), No. 7732, p. 546.

[2] B. Gludovatz, A. Hohenwarter, D. Catoor, E.H. Chang, E.P. George, and R.O. Ritchie, A fracture-resistant high-entropy alloy for cryogenic applications, *Science*, 345(2014), No. 6201, p. 1153.

[3] T.W. Zhang. S.G. Ma. D. Zhao. Y.C. Wu. Y. Zhang. Z.H. Wang and J.W. Qiao, Simultaneous enhancement of strength and ductility in a NiCoCrFe high-entropy alloy upon dynamic tension: Micromechanism and constitutive modeling, *Int. J. Plast.*, 124(2020), p. 226.

[4] G. Qin, S. Wang, R.R. Chen, X. Gong, L. Wang, Y.Q. Su, J.J. Guo, and H.Z. Fu, Microstructures and mechanical properties of Nb-alloyed CoCrCuFeNi high-entropy alloys, *J. Mater. Sci. Technol.*, 34(2018), No. 2, p. 365.

[5] E.P. George, D. Raabe, and R.O. Ritchie, High-entropy alloys, *Nat. Rev. Mater.*, 4(2019), No. 8, p. 515.

[6] C.D. Gómez-Esparza, R. Peréz-Bustamante, J.M. Alvarado-Orozco, J. Muñoz-Saldaña, R. Martínez-Sánchez, J.M. Olivares-Ramírez, and A. Duarte-Moller, Microstructural evaluation and nanohardness of an AlCoCuCrFeNiTi high-entropy alloy, *Int. J. Miner. Metall. Mater.*, 26(2019), No. 5, p. 634.

[7] X. Yang and Y. Zhang, Prediction of high-entropy stabilized solid-solution in multi-component alloys, *Mater. Chem. Phys.*, 132(2012), No. 2-3, p. 233.

[8] Y.J. Liang, L.J. Wang, Y.R. Wen, *et al*., High-content ductile coherent nanoprecipitates achieve ultrastrong high-entropy alloys, *Nat. Commun.*, 9(2018), No. 1, p. 4063.

[9] L.L. Wang, Z.A. Munir, and Y.M. Maximov, Thermite reactions: Their utilization in the synthesis and processing of materials, *J. Mater. Sci.*, 28(1993), No. 14, p. 3693.

[10] R.W. Cahn, Self-propagating high-temperature synthesis, *Adv. Mater.*, 2(1990), No. 6-7, p. 314.

[11] W.R. Wang, H.F. Xie, L. Xie, X. Yang, J.T. Li, and Q. Peng, Fabrication of ceramics/high-entropy alloys gradient composites by combustion synthesis in ultra-high gravity field, *Mater. Lett.*, 233(2018), p. 4.

[12] G.H. Liu, J.T. Li, K.X. Chen, G. He, Z.C. Yang, and S.B. Guo, High-gravity combustion synthesis of W–Cr alloys with improved hardness, *Mater. Chem. Phys.*, 182(2016), p. 6.

[13] G.H. Liu, J.T. Li, Z.C. Yang, S.B. Guo, and Y.X. Chen, High-gravity combustion synthesis and *in situ* melt infiltration: A new method for preparing cemented carbides, *Scripta Mater.*, 69(2013), No. 8, p. 642.

[14] G.H. Liu, J.T Li, and Y.X. Chen, Phase separation in melt-casting of ceramic materials by high-gravity combustion synthesis, *Mater. Chem. Phys.*, 133(2012), No. 2-3, p. 661.

[15] P.L. Mai, W.L. Fang, G.H. Liu, Y.X. Chen, S.L. He, and J.T. Li, Preparation of W–Ni graded alloy by combustion synthesis melt-casting under ultra-high gravity, *Mater. Lett.*, 65(2011), No. 23-24, p. 3496.

[16] P.F. Paradis and T. Ishikawa, Surface tension and viscosity measurements of liquid and undercooled alumina by containerless techniques, *Jpn. J. Appl. Phys.*, 44(2005), No. 7A, p. 5082.

[17] B. Glorieux, F. Millot, J.C. Rifflet, and J.P. Coutures, Density of superheated and undercooled liquid alumina by a contactless method, *Int. J. Thermophys.*, 20(1999), No. 4, p. 1085.

[18] L. Battezzati and A.L. Greer, The viscosity of liquid metals and alloys, *Acta. Metall.*, 37(1989), No. 7, p. 1791.

[19] T. Iida and R. I. L. Guthrie, *The Physical Properties of Liquid Metals*, Oxford Science Publications, Oxford, 1988.